RSC Advances

PAPER

View Article Online
View Journal | View Issue

Cite this: *RSC Adv.*, 2015, **5**, 49791

Adsorption of Cr(VI) onto a magnetic $CoFe_2O_4$/MgAl-LDH composite and mechanism study†

Lin Deng, Zhou Shi* and Xiaoxu Peng

Magnetic materials as adsorbents can provide effective removal and quickly separate pollutants in wastewater treatment. A magnetic $CoFe_2O_4$/MgAl-LDH composite was successfully synthesized through a low saturation coprecipitation method. The adsorption behaviors of Cr(VI) from an aqueous solution by $CoFe_2O_4$/MgAl-LDH were investigated. The adsorbents were characterized using scanning electron microscopy (SEM), N_2 adsorption–desorption isotherms, X-ray diffraction (XRD), Fourier transform infrared spectroscopy (FTIR) and X-ray photoelectron spectroscopy (XPS). Kinetic and equilibrium studies indicated that the experimental data of Cr(VI) adsorption were best described by pseudo-second-order kinetic and Langmuir models. The maximum adsorption capacity of $CoFe_2O_4$/MgAl-LDH for Cr(VI) was found to be 72.4 mg g^{-1} at an equilibrium time of 300 min and temperature of 283 K. Evaluation of the thermodynamics parameters ($\Delta H < 0$, $\Delta S < 0$ and $\Delta G < 0$) revealed the adsorption process was exothermic and spontaneous. The mechanism study showed that the adsorption of Cr(VI) onto $CoFe_2O_4$/MgAl-LDH likely involved adsorption/surface complexation and an ion exchange interaction. This study demonstrated that the magnetic $CoFe_2O_4$/MgAl-LDH composite was an effective adsorbent for Cr(VI) removal with quick separation.

Received 7th April 2015
Accepted 29th May 2015

DOI: 10.1039/c5ra06178d

www.rsc.org/advances

1. Introduction

Effluents containing hexavalent chromium Cr(VI) generated from electroplating, textile, metal finishing, mining, leather tanning and pigment manufacturing have become a major concern due to its high toxicity, carcinogenic and mutagenic properties to both the environment and living organisms.[1–4] To prevent the harmful impact of Cr(VI) on public health, many countries around the world have regulations on the maximum permissible concentration of Cr(VI) in natural or drinking water. A maximum allowable limit of 0.05 mg L^{-1} for total chromium has been set by the World Health Organization (WHO) drinking water guidelines,[5] and the permissible Cr(VI) concentration in drinking water is 0.05 mg L^{-1} in China.[6] Therefore, to protect the environment and human health, it has become imperative to find an effective way to remove Cr(VI) from wastewaters to an acceptable threshold before releasing them into water bodies.

Various physicochemical and biological techniques have been developed to eliminate Cr(VI) from industrial wastewaters including chemical precipitation,[7] ion exchange,[8] membrane filtration,[9] solvent extraction,[10] adsorption[2–4,11] and biological processes,[12] *etc.* Among these techniques, adsorption method has attract much attention due to its significant advantages such as simplicity of design and operation, cost-effective, high efficiency, recycle of adsorbent, and no secondary pollution.[13] The key to practical application of adsorption requires the adsorbent with high surface area for more binding sites and strong adsorption affinity to adsorbate. Thus, many types of adsorbents such as low-cost or easily available clays, carbon materials, nanomaterials, biomaterials, by-products and waste materials have been investigated extensively and systematically for the removal of Cr(VI) from aqueous solution.[14–17]

Layered double hydroxides (LDHs) is an anionic clay, whose chemical composition can be generally expressed as $[M_{1-x}^{2+}M_x^{3+}(OH)_2]^{x+}[A_{x/n}^{n-}]^{x-}\cdot mH_2O$, where M^{2+} and M^{3+} represent divalent metal cations (Mg^{2+}, Ni^{2+}, Zn^{2+}, Ca^{2+}, Co^{2+}, Cu^{2+} or Cd^{2+}) and trivalent metal cations (Al^{3+}, Fe^{3+}, Cr^{3+} or V^{3+}), respectively, A^{n-} represent the interlayer anions (CO_3^{2-}, NO_3^- or Cl^-) that balance the positive charge on the layers, and x is donated as the molar ratio of $M^{2+}/(M^{2+} + M^{3+})$.[18,19] In recent years, LDHs such as LiAl-LDH,[20] MgAl-LDH,[21] Fe^{2+}-doped MgAl-LDH,[22] and ZnAl-LDH,[23] have been detailed investigated for the removal of Cr(VI) ions from aqueous solution, and the LDHs have exhibited great adsorption capacity for Cr(VI) because of its high surface area, layered structure, and interlayer anion mobility of its A^{n-} host.[24] However, LDHs suffer from separation convenience, preventing them from industrial application scopes greatly.[25,26] To overcome this issue, it is necessary to explore novel LDHs-based adsorbents, which possess higher adsorption capacity and separation property.

Key Laboratory of Building Safety and Energy Efficiency, Ministry of Education, Department of Water Engineering and Science, College of Civil Engineering, Hunan University, Yuelu Mountain, Changsha 410082, Hunan, PR China. E-mail: 369329062@qq.com

† Electronic supplementary information (ESI) available. See DOI: 10.1039/c5ra06178d

Magnetic materials have been introduced into the adsorbent recently, and the magnetic separation method has been considered as high separation efficiency, low cost and convenient technique in comparison with the traditional separation methods such as precipitation, centrifugation or filtration. Porous materials can provide effective sites for adsorption process; moreover, their irregular and wide pore size distribution will be beneficial for the adsorption. Stimulated by the promising application of the hybrid systems with porous materials and magnetic particles with characteristics of high efficiency, fast adsorption rate and facile separation, a few reports have been made in preparing of different types of magnetic porous adsorbents.[27,28] Iron oxide (Fe_3O_4) is the most commonly used magnetic material recently due to its low cost and low toxicity. Mohammadi *et al.*[29] synthesized superparamagnetic sodium alginate-coated Fe_3O_4 nanocomposites (Alg-Fe_3O_4) by *in situ* coprecipitation method, and the adsorbent exhibited a maximum adsorption capacity of 47.84 mg g^{-1} for adsorption of malachite green dye onto Alg-Fe_3O_4. Fang *et al.*[30] prepared an ethylenediamine (EDA) functionalized Fe_3O_4 (EDA-Fe_3O_4) for removing Cr(VI) from aqueous solution, and the maximum adsorption capacity was found to be 81.5 mg g^{-1} at pH 2.0. Li *et al.*[31] reported the recyclable CNTs/Fe_3O_4 magnetic composites synthesized through a facile hydrothermal method, and the adsorbent showed magnetic separability and strong adsorption behaviors in the treatment of bisphenol A (BPA) in aqueous solution. However, Fe_3O_4 is susceptible to acid conditions, which might decrease the magnetic separability of adsorbents; moreover some reactants (such as ethylenediamine) for preparation of Fe_3O_4 may be harm to the environment.[32]

Spinel ferrites (*e.g.* $MnFe_2O_4$, $CoFe_2O_4$, $NiFe_2O_4$, $CuFe_2O_4$ and $MgFe_2O_4$) have been widely used in electrical and practical applications of information storage system, magnetocaloric refrigeration, and ferrofluid technology; and they have also been employed for water purification for the last several years, but their adsorption efficiency was not satisfactory.[33,34] In this study, $CoFe_2O_4$ was selected as the magnetic core. To the best of our knowledge, the $CoFe_2O_4$/MgAl-LDH composite composed of $CoFe_2O_4$ as the magnetic core coated with the nanostructured crystalline MgAl-LDH, especially in the field of application of the adsorbent for removing Cr(VI) from aqueous solution, has rarely been reported before.

The objective of this study was to evaluate the potential of using $CoFe_2O_4$/MgAl-LDH to remove Cr(VI) from aqueous solution. The adsorption properties as functions of varied operational conditions (solution pH, contact time, initial Cr(VI) concentration, temperature and coexisting ions) were investigated systematically. Adsorption kinetics, isotherms and thermodynamics were studied to expound the specific adsorption mechanism of Cr(VI) onto $CoFe_2O_4$/MgAl-LDH. The physical structure and chemical properties of the as-prepared $CoFe_2O_4$/MgAl-LDH were characterized in detail by scanning electron microscope (SEM), N_2 adsorption–desorption isotherms, X-ray diffraction (XRD), Fourier transform infrared spectroscopy (FTIR) and X-ray photoelectron spectroscopy (XPS).

2. Materials and methods

2.1 Materials

The chemicals, $CoCl_2 \cdot 4H_2O$, $FeSO_4 \cdot 7H_2O$, $Al(NO_3)_3 \cdot 9H_2O$, $Mg(NO_3)_2 \cdot 6H_2O$, Na_2CO_3, NaOH, HCl, ammonia, ethylene glycol and ethyl alcohol were purchased from Tianjin Kemiou Chemical Reagent Co., Ltd., China. $K_2Cr_2O_7$ were supplied from Tianjin Hengxing Chemical Reagent Co., Ltd., China. All of the reagents were of analytical grade and were used as received without any further purification. Doubly distilled deionized water was used throughout this study. Various Cr(VI) solutions with different concentrations were prepared by dissolving $K_2Cr_2O_7$ in deionized water.

2.2 Preparation of magnetic $CoFe_2O_4$/MgAl-LDH composite

The $CoFe_2O_4$ nanoparticles were synthesized by hydrothermal synthesis method. 1.112 g of $FeSO_4 \cdot 7H_2O$ and 0.4758 g $CoCl_2 \cdot H_2O$ were dissolved in a mixture of 60 mL of ethylene glycol solvent and 40 mL deionized water, followed by the addition of 4 mL of ammonia solution (NH_3H_2O). The above mixture was stirred vigorously for 1 h and then poured into a 100 mL Teflon-lined autoclave. The autoclave was heated to and maintained at 180 °C for 24 h. After cooling to room temperature, the precipitate was washed several times with deionized water and ethanol, and dried at 60 °C for 12 h. The ethylene glycol serves as not only a high boiling point (197.3 °C) solvent to keep the volume of the reaction solution constant during the hydrothermal synthetic process being carried at relatively high temperature, but also a phase to prevent the newly formed reaction product, $CoFe_2O_4$ nanoparticles, from conglomerating. Ammonia solution (NH_3H_2O) has two functions: first, NH_3H_2O is an oxidizing agent to oxidize Fe^{2+} to Fe^{3+}. Second, NH_3H_2O as a weak base can help Co^{2+} and Fe^{3+} to precipitate as hydroxides and then to form $CoFe_2O_4$ nanoparticles through dehydration in the hydrothermal synthetic process.

The magnetic $CoFe_2O_4$/MgAl-LDH composite was synthesized through low saturation coprecipitation method. A certain amount of prepared $CoFe_2O_4$ (0.5 g) was ultrasonically dispersed into 150 mL deionized water in 500 mL beaker for 20 min to obtain a uniform suspension, and then the beaker was transferred into a water batch at 60 °C with vigorous stirring. Meanwhile, a salt solution (100 mL) containing 0.125 mol L^{-1} $Al(NO_3)_3 \cdot 9H_2O$ and 0.25 mol L^{-1} $Mg(NO_3)_2 \cdot 6H_2O$ was dropwise added into the suspension, and an alkaline solution (100 mL) containing 3.375 g NaOH and 2.645 g Na_2CO_3 was added simultaneously to keep the pH at 10.0–10.5. After complete addition of the two solutions, the suspension was aged for 8 h, followed by washing with deionized water until the effluent solution is neutral. The resulting product was dried at 60 °C for 12 h.

2.3 Characterization methods

The morphologies of adsorbents were determined by Hitachi S-4800 SEM operating at 5 kV. The specific surface area and pore diameter measurements were carried out by nitrogen adsorption at 77 K using an automated gas sorption analyzer

(Quantachrome Instruments, QuadraSorb Station 1). XRD data were collected on a Rigaku D/Max-2500 powder diffractometer with Cu Kα radiation with a scan step of 0.02°. Infrared spectra of the adsorbents were recorded using a FT-IR spectrometer (Thermo Nicolet, Nexus-470, USA) at 400–4000 cm^{-1}. XPS measurements were performed on ESCALab220i-XL electron spectrometer from VG Scientific using 300 W Al Kα radiations.

2.4 Adsorption experiments

The adsorption of Cr(VI) from aqueous solutions onto the $CoFe_2O_4$/MgAl-LDH was studied in a batch system. In each adsorption experiment, 50 mL of Cr(VI) solution with known concentration was put into a 120 mL polyethylene bottles. The solution pH measured by a pH meter (Orion Research. Inc, Model 868, USA) was adjusted to a predetermined value with 0.1 mol L^{-1} HCl or 0.1 mol L^{-1} NaOH, and 0.15 g $CoFe_2O_4$/MgAl-LDH was added into the above solution. Subsequently, the resulting mixture was stirred in a thermostatic water bath shaker to reach equilibrium except kinetic experiments. At the end of each experiment, the supernatant was filtered using 25 mm 0.45 μm membrane filter, and the filtrate was then analyzed for the residual Cr(VI) concentration in solution. The residual Cr(VI) concentration in solution was determined with 1,5-diphenylcarbohydrazide spectrophotometric method using an ultraviolet spectrophotometer (Hitachi, U-3900, Japan). Blank experiments were run in parallel on Cr(VI) solutions, without addition of adsorbent, for the sake of comparison. All tests were carried out in triplicate, and their mean values were used in analyzing the data.

The removal efficiency (R, %) and the amount of Cr(VI) adsorbed at time t (q_t, mg g^{-1}) were calculated according to the formula:

$$R = \frac{C_0 - C_t}{C_0} \times 100\% \quad (1)$$

$$q_t = \frac{(C_0 - C_t) \times V}{m} \quad (2)$$

where C_0 (mg L^{-1}) and C_0 (mg L^{-1}) are the liquid phase concentration of Cr(VI) at initial and time t (min), respectively. V (L) is the volume of Cr(VI) solution, m (g) is the mass of the adsorbent.

3. Results and discussion

3.1 Characterization of $CoFe_2O_4$/MgAl-LDH composite

Nitrogen adsorption–desorption isotherms were recorded to examine the surface and pore structure of MgAl-LDH, $CoFe_2O_4$, $CoFe_2O_4$/MgAl-LDH before and after Cr(VI) adsorption. Fig. S1† depicted the results of nitrogen adsorption–desorption isotherms. All of the four isotherm curves exhibited the representative type-IV curves with hysteresis loops, indicating the uniform mesoporous structure of the four samples. Table 1 showed the specific surface area, pore volume, and average pore diameter of the adsorbents.

Obviously, compared with the $CoFe_2O_4$, the introduction of MgAl-LDH led to a distinct increase in BET surface area (from 15.12 to 120.75 m^2 g^{-1}), pore volume (from 0.074 to 0.756 cm^3 g^{-1}) and pore diameter (from 3.83 to 18.65 nm) of $CoFe_2O_4$/MgAl-LDH, which were beneficial to the adsorption of Cr(VI). The decrease in BET surface area, pore volume and pore diameter of $CoFe_2O_4$/MgAl-LDH after Cr(VI) adsorption indicated that Cr(VI) ions was probably adsorbed by the adsorbent into its pores and developed a layer of Cr(VI) substance on the surface. This was also in accordance with SEM results shown in Fig. S2,† in which the adsorbent after Cr(VI) adsorption became more abnormal and a great deal of crystal adhered to the adsorbent surface.

XRD of MgAl-LDH, $CoFe_2O_4$, $CoFe_2O_4$/MgAl-LDH before and after Cr(VI) adsorption was carried out to identify the phase structure of adsorbents. It was observed in Fig. 1a that MgAl-LDH exhibited diffraction peaks at $2\theta = 11.72°$, 23.58°, 34.99°, 39.56°, 47.10°, 60.90° and 62.21°, which could be assigned to the (003), (006), (009), (015), (018), (110) and (113) planes of Mg/Al-LAH nanoplates (JCPDS: 89-0460).[35] The diffraction peaks of (009), (015), (018), (110) and (113) had relatively low intensities, while peaks of (003) and (006) were especially strong, indicating that the crystal grew along a certain axis. Fig. 1b showed the XRD patterns of $CoFe_2O_4$. The diffraction signals located at (220), (311), (400), (422), (511) and (440) were ascribed to the characteristics peaks of single phase cubic spinel structure of $CoFe_2O_4$ (JCPDS: 22-1086).[34] The intensities of the characteristic reflections for both MgAl-LDH and $CoFe_2O_4$ phases in $CoFe_2O_4$/MgAl-LDH composite were not obviously changed compared to those in pure MgAl-LDH and $CoFe_2O_4$. Moreover, there were no other characteristic peaks detected in the XRD patterns of the adsorbent as shown in Fig. 1c, demonstrating that the synthesized adsorbent was a composite of MgAl-LDH and $CoFe_2O_4$ and the combination was probably a physical process. After adsorption of Cr(VI) from aqueous solution, the layered structure of the adsorbent was reconstructed (Fig. 1d). However, its XRD patterns were in good agreement with the characteristic peaks of $CoFe_2O_4$, indicating that the adsorption of Cr(VI) using $CoFe_2O_4$/MgAl-LDH was attributed to the sites provide by MgAl-LDH in the composite.

3.2 Effect of solution pH on Cr(VI) adsorption

Solution pH plays an important role in Cr(VI) adsorption owing to its effect not only on the degree of speciation and ionization of Cr(VI) but also on surface charge of the adsorbent. Fig. 2 illustrated the results of Cr(VI) adsorption by $CoFe_2O_4$/MgAl-LDH with the initial solution pH ranging from 2.0 to 11.0 at initial Cr(VI) concentration of 50 mg L^{-1}. It was observed that the adsorbent can be quickly separated from the aqueous solution by an external magnet before and after adsorption process. The amount of Cr(VI) adsorbed on $CoFe_2O_4$/MgAl-LDH was highly pH dependent, and the q_e value decreased gradually from 16.4 to 1.2 mg g^{-1} with increasing solution pH from 2.0 to 11.0.

The result could be explained by the pH_{zpc} of the adsorbent, which was illustrated in Fig. S3.† The corresponding pH value of the intersection point (intersection of the two curves of the pH_{final} *versus* $pH_{initial}$) was 8.8, *i.e.* the pH of the $CoFe_2O_4$/MgAl-

Table 1 Comparison of BET surface areas, pore volumes and pore diameters of MgAl-LDH, $CoFe_2O_4$, $CoFe_2O_4$/MgAl-LDH, $CoFe_2O_4$/MgAl-LDH after Cr(VI) adsorption

Adsorbent	BET surface area ($m^2\ g^{-1}$)	Pore volume ($cm^3\ g^{-1}$)	Average pore diameter (nm)
MgAl-LDH	143.60	0.963	15.48
$CoFe_2O_4$	15.12	0.074	3.83
$CoFe_2O_4$/MgAl-LDH	120.75	0.756	18.85
$CoFe_2O_4$/MgAl-LDH after Cr(VI) adsorption	7.23	0.020	5.42

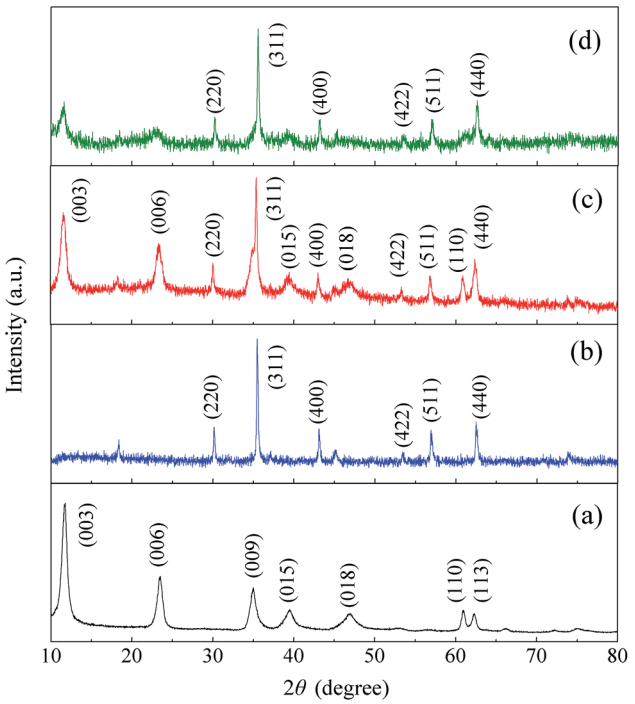

Fig. 1 XRD patterns of (a) MgAl-LDH, (b) $CoFe_2O_4$, (c) $CoFe_2O_4$/MgAl-LDH, and (d) $CoFe_2O_4$/MgAl-LDH after Cr(VI) adsorption.

LDH composite was 8.8. It is reported that Cr(VI) exists in species of H_2CrO_4, $HCrO_4^-$, CrO_4^{2-}, and $Cr_2O_7^{2-}$ at different ratios in aqueous solution, depending on the pH of the system.[3,14] At pH < 8.8, a lower solution pH caused the adsorbent surface to carry a positive charge due to protonation of the adsorbent surface,[22] and thus would more significantly attract the anions of Cr(VI). Moreover, the predominant Cr(VI) species of $HCrO_4^-$ was gradually converted to CrO_4^{2-} with an increase of solution pH. However, the adsorption free energy of $HCrO_4^-$ (−2.5 to −0.6 kcal mol^{-1}) was higher than that of CrO_4^{2-} (−2.1 to −0.3 kcal mol^{-1}),[3] thus $HCrO_4^-$ was more favorable for adsorption than CrO_4^{2-}. This could be further explained by the curve of the equilibrium pH *versus* the initial pH as depicted in Fig. 2, where the pH at equilibrium was found to be higher than the initial solution pH due to the decrease of H^+ ions concentration by the formation of $HCrO_4^-$ from CrO_4^{2-}. At solution pH > 8.8, the surface of the adsorbent became negatively charged due to deprotonation. Thus electrostatic repulsion between the negatively charged Cr(VI) species and the negatively charged adsorption sites on the adsorbent would increase. This would result in a release of the adsorbed $HCrO_4^-$ and CrO_4^{2-}. Moreover, the competition of OH^- ions for adsorption sites with Cr(VI) species increased with the increase of pH, resulting in a decrease in Cr(VI) uptake. Fig. 2 showed that the equilibrium pH was lower than the initial pH in the alkaline solutions, which was attributed to the OH^- ions concentration decreased by competing for adsorption sites with CrO_4^{2-}. Accordingly, pH value at 2 was an ideal parameter in this study.

3.3 Adsorption kinetics

Effect of initial concentration on Cr(VI) adsorption using $CoFe_2O_4$/MgAl-LDH was investigated by carrying out the experiments at different initial concentrations (50, 100 and 200 mg L^{-1}) and varying the contact time (Fig. 3). With increasing concentration from 50 to 200 mg L^{-1}, the equilibrium time increased from 90 to 300 min. As depicted in the figure, the adsorption rate was very high due to the availability of abundant adsorption sites on the surface of $CoFe_2O_4$/MgAl-LDH and the large concentration gradient between the fluid film around the adsorbent particle. After a lapse of time, the remaining vacant adsorption sites were difficult to be occupied because of repulsive forces between the Cr(VI) molecules on the solid and bulk phases, resulting in a low adsorption rate until the achievement of equilibrium. The uptake amount of Cr(VI) at

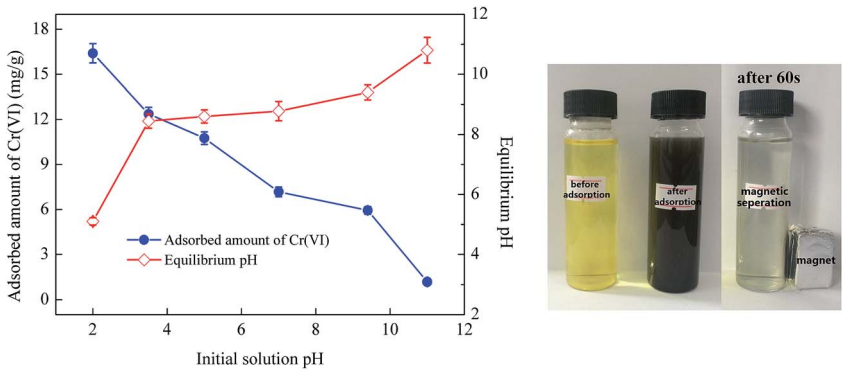

Fig. 2 Effect of initial solution pH on Cr(VI) adsorption and equilibrium pH using $CoFe_2O_4$/MgAl-LDH.

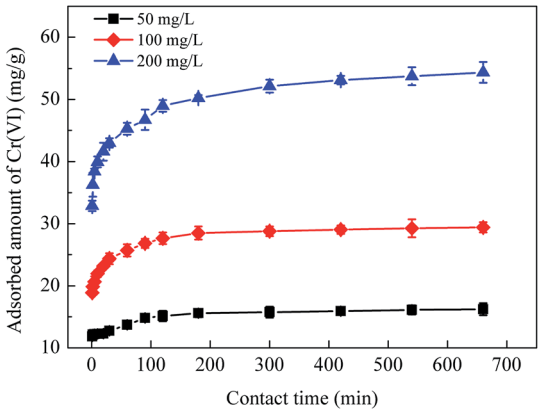

Fig. 3 Effect of contact time on Cr(VI) adsorption using $CoFe_2O_4$/MgAl-LDH for initial Cr(VI) concentrations of 50, 100 and 200 mg L^{-1}.

equilibrium was observed to increase immensely from 16.24 to 54.37 mg g^{-1} with initial Cr(VI) concentration increased from 50 to 200 mg L^{-1}. High initial Cr(VI) concentration expanded the effective contact area with adsorbent and provided essential driving force to transcend the resistance to the mass transfer of Cr(VI) on interface.

To analyze the mechanism and rate-controlling step in the overall adsorption process of Cr(VI) onto $CoFe_2O_4$/MgAl-LDH, the experimental data was fitted using pseudo-first-order and pseudo-second-order kinetic models,[36,37] with the respective kinetics equations defined as follows:

$$\log(q_e - q_t) = \log q_e - \frac{k_1}{2.303}t \quad (3)$$

$$\frac{t}{q_t} = \frac{1}{k_2 q_e^2} + \frac{1}{q_e}t \quad (4)$$

where q_e (mg g^{-1}) and q_t (mg g^{-1}) are the amounts of Cr(VI) adsorbed at equilibrium time and at any instant of time, t, respectively, k_1 (min^{-1}) and k_2 (g (mg^{-1} min^{-1})) are the rate constant of pseudo-first-order and pseudo-second-order model, respectively. The values of k_1 and k_2 can be determined from the slope of the linear plot of $\log(q_e - q_t)$ *versus* t and t/q_t *versus* t, respectively.

Table 2 summarized the calculated kinetic parameters obtained by the linear regression for the two models (Fig. 4a and b). The correlation coefficient (R^2) obtained from the pseudo-second-order kinetic model ($R^2 > 0.999$) was higher than that obtained from the pseudo-first-order kinetic model (R^2 was in the range of 0.9406–0.9721), suggesting that the adsorption of Cr(VI) onto $CoFe_2O_4$/MgAl-LDH could be well described by the pseudo-second-order kinetic model. Besides, the experimental equilibrium capacity ($q_{e,exp}$) were very close to the calculated equilibrium capacity ($q_{e,cal}$) for this model. The fitness of the pseudo-second-order kinetic model implied that the rate-limiting step may be chemical adsorption involving valency forces through sharing or exchange of electrons between the adsorbent and Cr(VI).[37] However at the same time, the initial rapid phase within the first 30 min may involve physical adsorption or exchange at the surface of the adsorbent.[36]

The adsorption on a porous adsorbent will generally have multi-step process. The intraparticle diffusion model proposed by Weber and Morris was also used to characterize the adsorption data. The plot of q_t *versus* $t^{1/2}$ at different initial Cr(VI) concentrations was depicted in Fig. 4. As observed, the plot exhibited a multi-straight-line nature, suggesting that more than one process affected the adsorption. The values of k_i and R^2 were shown in Table 2. The data represented three periods of adsorption including the rapid section (stage 1 and stage 2) and the stabilization section (stage 3). The initial rapid stages were ascribed to the passage of Cr(VI) into the pores of $CoFe_2O_4$/MgAl-LDH corresponding to the boundary layer diffusion. The final stage was the residual adsorption process, indicating that the adsorption reached ultimate equilibrium. Additionally, Table 2 also represented that the rate constants ($k_{i,1}$, $k_{i,2}$ and $k_{i,3}$) increased significantly in all adsorption regions with increasing initial Cr(VI) concentration from 50 to 200 mg L^{-1}, suggesting that the driving force increased as the Cr(VI) concentrations was increased.

3.4 Adsorption isotherms and thermodynamic studies

Adsorption isotherms are usually used to describe the relationship between the adsorbate concentration in solution and the adsorbate amount adsorbed by the unit mass of adsorbent at a constant temperature at equilibrium. Equilibrium study in adsorption is fundamentally important for the predictive modeling procedures for analyzing and designing an adsorption system. Fig. 5 showed the effect of temperature on the uptake of Cr(VI) by $CoFe_2O_4$/MgAl-LDH. With increase in temperature from 283 to 323 K, the adsorbed amount of Cr(VI) decreased gradually for all the concentrations. This may be attributed to desorption caused by an increased available thermal energy. Higher temperature induced higher mobility of the solute causing desorption.[38] Moreover, a decrease in q_e value

Table 2 Comparison of rate constants calculated based on respective pseudo-first-order, pseudo-second-order, and intraparticle diffusion kinetic models

		Pseudo-first-order			Pseudo-second-order			Intraparticle diffusion					
C_0	$q_{e,exp}$	k_1	$q_{e,cal}$	R^2	k_2	$q_{e,cal}$	R^2	$k_{i,1}$	R_1^2	$k_{i,2}$	R_2^2	$k_{i,3}$	R_3^2
50	16.23	0.0046	3.68	0.9475	0.0106	16.26	0.9997	0.47	0.4925	0.39	0.9512	0.059	0.9844
100	29.40	0.0076	6.89	0.9406	0.0066	29.49	0.9998	1.34	0.9707	0.59	0.9702	0.076	0.9914
200	54.37	0.0060	14.96	0.9721	0.0024	54.41	0.9993	3.03	0.8328	0.99	0.9814	0.26	0.9924

with an increase in temperature indicated an exothermic reaction nature of the adsorption. Similar trends were also reported by Sadaoui *et al.*[39] and Gupta *et al.*[40] It was found that the maximum adsorption capacities of Cr(VI) by micellar compounds decreased from 17.89 to 13.85 mg g^{-1} with increasing temperature from 30 to 45 °C; Gupta *et al.* also reported that the uptake of Cr(VI) decreased from 14.7 to 12.8 mg g^{-1} with the rise in temperature from 303 to 323 K (30 to 50 °C).

To examine the relationship between Cr(VI) and the adsorbent at equilibrium and to search the maximum adsorption capacity of the adsorbent, the experimental data were analyzed by the well-known Langmuir and Freundlich isotherm models,[41] which are usually expressed by the following equations:

$$q_e = \frac{bq_m C_e}{1 + bC_e} \quad (5)$$

$$q_e = K_f C_e^{1/n} \quad (6)$$

where q_e (mg g^{-1}) and C_e (mg L^{-1}) are the adsorption capacity and the equilibrium concentration of the adsorbate in solution, respectively, q_m (mg g^{-1}) is the maximum adsorption capacity corresponding to the complete monolayer coverage, b (L mg^{-1}) is the Langmuir constant related to the affinity of binding sites, and K_f and $1/n$ are Freundlich constants related to adsorption capacity and adsorption intensity, respectively.

The results obtained from the isotherms are summarized in Table 3. It was found that Langmuir model could be better described the adsorption process for the higher correlation coefficients ($R^2 > 0.99$) compared with Freundlich model, suggesting the homogeneous adsorption of Cr(VI) on $CoFe_2O_4$/MgAl-LDH and the adsorbed Cr(VI) formed a mono-molecular layer on the surface of the adsorbent. The maximum adsorption capacity of the adsorbent determined from the Langmuir model was found to be 72.4 mg g^{-1} for temperatures of 283 K. It is important to note that the adsorption capacity of Cr(VI) exhibited by the $CoFe_2O_4$/MgAl-LDH (72.4 mg g^{-1}) is higher than some other hydrotalcite materials such as uncalcined carbonate–Mg–Al LDHs (17 mg g^{-1}), Li/Al LDH (9.98 mg g^{-1}), calcined Mg–Al–Zr (24 mg g^{-1}), uncalcined Mg–Al LDHs (16.3 mg g^{-1}), HLCs (25.7 mg g^{-1}), calcined MgAl–CO_3-HT (33.4–44.7 mg g^{-1}) and uncalcined chloride–Zn–Al LDHs (23.3 mg g^{-1}) (as shown in Table 4), which expressed a potential in the application of Cr(VI) removal. Decreasing in Langmuir

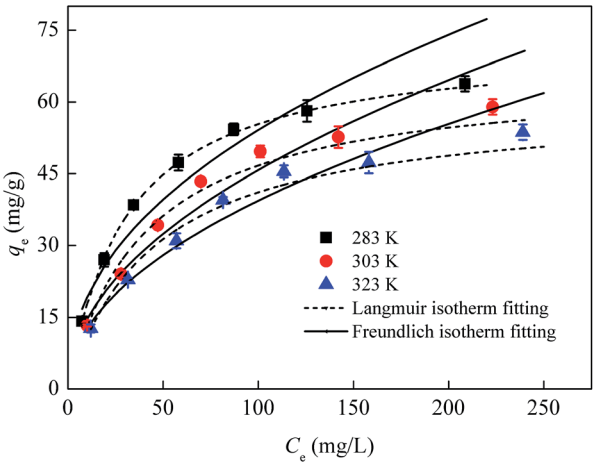

Fig. 5 Adsorption isotherm of Cr(VI) on $CoFe_2O_4$/MgAl-LDH at temperatures of 283, 303, 323 K.

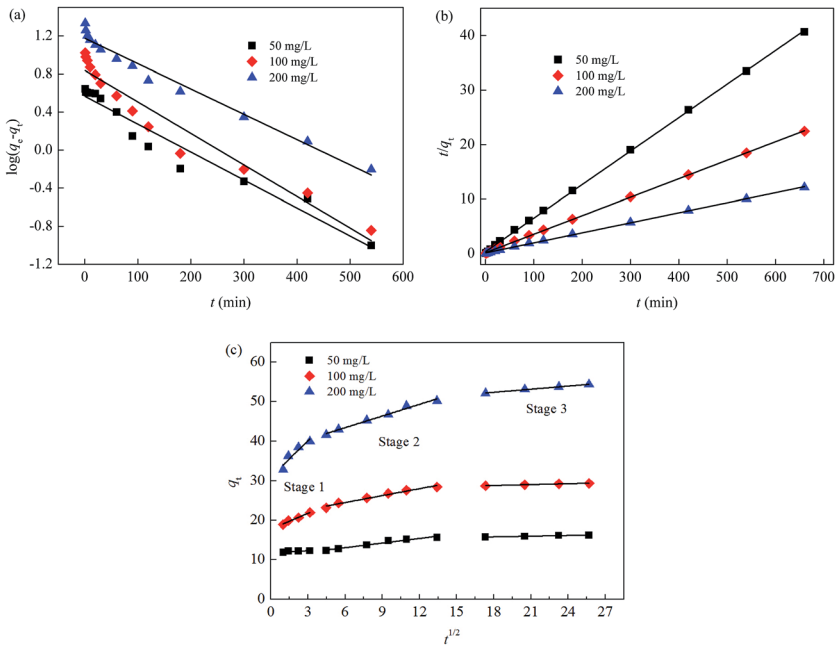

Fig. 4 Intraparticle diffusion model fitting of adsorption kinetic of Cr(VI) on $CoFe_2O_4$/MgAl-LDH.

Table 3 Parameters of Langmuir and Freundlich isotherms for adsorption of Cr(VI) onto $CoFe_2O_4$/MgAl-LDH

	Langmuir isotherm				Freundlich isotherm		
T (K)	q_m (mg g^{-1})	K_L (L mg^{-1})	R_L	R^2	K_f (mg g^{-1})	$1/n$	R^2
283	72.4	0.032	0.0725–0.385	0.9995	6.76	0.452	0.9440
303	65.7	0.024	0.0943–0.455	0.9908	4.64	0.496	0.9641
323	59.8	0.022	0.102–0.476	0.9929	4.05	0.494	0.9720

constant b with temperature confirmed the exothermic nature of the adsorption process.

The essential characteristics of the Langmuir adsorption isotherm can be expressed by means of a dimensionless constant, R_L, which is referred to as separation factor or equilibrium parameter and can be defined as:

$$R_L = \frac{1}{1 + C_0 b} \quad (7)$$

The R_L value suggests the type of isotherm to be unfavorable ($R_L > 1$), linear ($R_L = 1$), favorable ($0 < R_L < 1$), irreversible ($R_L = 0$). From Table 3, the R_L values were found to be in the range of 0 to 1, suggesting the favorable adsorption of Cr(VI) on $CoFe_2O_4$/MgAl-LDH.

Thermodynamic consideration of an adsorption process are necessary to deduce whether the process is spontaneous or not, and provide in-depth information about internal energy changes that are associated with the adsorption. Experimental data of Cr(VI) adsorbed at equilibrium at different temperatures was used to evaluate the thermodynamic parameters such as enthalpy change (ΔH), Gibbs free energy change (ΔG), and entropy change (ΔS) for the adsorption system by the following equations:

$$\Delta G = -RT \ln K_L \quad (8)$$

$$\Delta G = \Delta H - T\Delta S \quad (9)$$

where K_L (L mol^{-1}) is the Langmuir constant. ΔH and ΔS can be calculated from the slope and intercept of van't Hoff plots of $\ln K_L$ *versus* $1/T$. The obtained ΔG, ΔH, and ΔS were listed in Table 5.

The negative values of ΔG at various temperatures (−1.14, −0.71 and −0.28 kJ mol^{-1} to 283, 303 and 323 K, respectively) demonstrated the feasibility and spontaneous nature of the adsorption process. The value of ΔG became more negative with the decrease in temperature, indicating that lower temperature facilitated adsorption of Cr(VI) onto $CoFe_2O_4$/MgAl-LDH. The negative value of ΔH (−7.18 kJ mol^{-1}) indicated that the reaction was exothermic; hence the uptake amount of Cr(VI) decreased with increasing temperature of the solution. The negative value ΔS (−21.36 J mol^{-1} K^{-1}) of Cr(VI) adsorption using $CoFe_2O_4$/MgAl-LDH corresponded to a decrease in randomness at the liquid/solid interface during the adsorption process.

3.5 Adsorption mechanisms

The adsorption experiments of $CoFe_2O_4$ for Cr(VI) were carried out, but it turned out that the $CoFe_2O_4$ had almost no adsorption capacity for Cr(VI) (data not shown). This result suggested that the adsorption of Cr(VI) using $CoFe_2O_4$/MgAl-LDH may be contributed to MgAl-LDH. To elucidate the interaction mechanisms between Cr(VI) ions and the adsorbent, FTIR analyses of MgAl-LDH, $CoFe_2O_4$, $CoFe_2O_4$/MgAl-LDH before and after Cr(VI) adsorption were performed.

The FTIR spectrum of MgAl-LDH showed characteristic bands related to the H-bonding stretching vibrations of OH groups in the brucite-like layer at 3441 cm^{-1} and the H_2O bending vibration at 1637 cm^{-1}. A band at 1362 cm^{-1} may be attributed to contamination by CO_3^{2-} ions in the MgAl-LDH synthesis.[21] The bands between 400 and 800 cm^{-1} could be related to the superposition of the characteristic vibrations of aluminum and magnesium oxides.[22] Fig. 6b exhibited the FTIR spectrum of $CoFe_2O_4$. The adsorption peaks at 590 and 410 cm^{-1} may be ascribed to the intrinsic vibration of the tetrahedral and octahedral sites in the $CoFe_2O_4$ particles.[47]

Table 4 The Cr(VI) adsorption capacity of $CoFe_2O_4$/MgAl-LDH compared with other hydrotalcite materials

Adsorbent	Adsorption capacity (mg g^{-1})	Reference
Uncalcined carbonate–Mg–Al LDHs	17	3
Li/Al LDH	9.98	21
Calcined Mg–Al–Zr (450 °C)	24	42
Uncalcined Mg–Al LDHs	16.3	43
HLCs	25.7	44
HLCs heated at 350 °C	25.8	
HLCs heated at 150 °C	28.5	
Calcined MgAl–CO_3-HT (CHT)	33.4–44.7	45
Uncalcined chloride–Zn–Al LDHs	23.3	46
$CoFe_2O_4$/MgAl-LDH	72.4	This work

Table 5 Values of thermodynamic parameters for adsorption of Cr(VI) onto $CoFe_2O_4$/MgAl-LDH

T (K)	$\ln K_L$	ΔG (kJ mol^{-1})	ΔH (kJ mol^{-1})	ΔS (J mol^{-1} K^{-1})
283	0.509	−1.14	−7.18	−21.36
303	0.222	−0.71		
323	0.135	−0.28		

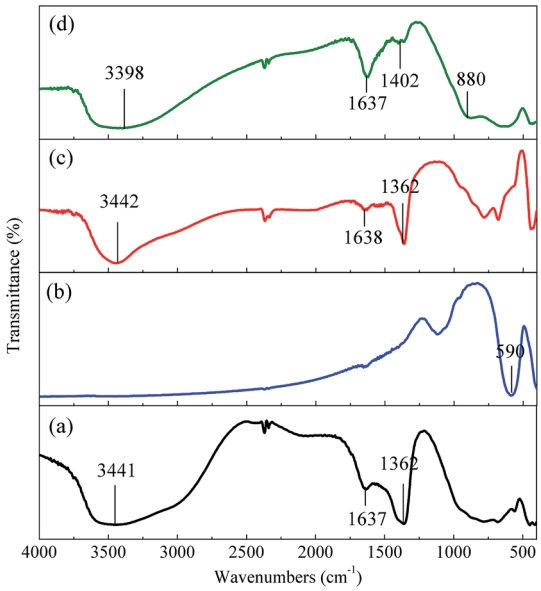

Fig. 6 FTIR spectra of (a) MgAl-LDH, (b) $CoFe_2O_4$, (c) $CoFe_2O_4$/MgAl-LDH, (d) $CoFe_2O_4$/MgAl-LDH after Cr(VI) adsorption.

However, the $CoFe_2O_4$ synthesized in this study did not show any bands related to the H-bonding stretching vibrations of the OH group, resulting in low adsorption capacity for Cr(VI). The FTIR spectrum of the $CoFe_2O_4$/MgAl-LDH composite illustrated in Fig. 6c was almost identical to that of the MgAl-LDH. As shown in Fig. 6d, the band at 3442 cm^{-1} shifted to 3398 cm^{-1} after adsorption of Cr(VI), suggesting that the bonded OH groups played an important role in Cr(VI) adsorption.[48] Additionally, the characteristic FTIR band of chromate due to mode ν_d(Cr–O), recorded at 890 cm^{-1} for free chromate,[22] appeared at 880 cm^{-1} for the $CoFe_2O_4$/MgAl-LDH sample after adsorption of Cr(VI). This indicated the interlayer NO_3^- ions were exchanged with Cr(VI) anions in solution.[21] The slight shift toward lower frequency from 890 to 880 cm^{-1} suggested that the Cr–O bond for $CoFe_2O_4$/MgAl-LDH-Cr was weaker than for the free chromate, which may be attributed to hydrogen bonding of the $HCrO_4^-$ with layer OH groups and interlayer H_2O molecules.

In order to give more detailed information about the adsorption mechanism, MgAl-LDH, $CoFe_2O_4$, $CoFe_2O_4$/MgAl-LDH before and after Cr(VI) adsorption were analyzed by the XPS. Compared to the typical XPS spectra of $CoFe_2O_4$ shown in Fig. S4,† the wide scan XPS spectra of $CoFe_2O_4$/MgAl-LDH before and after Cr(VI) adsorption exhibited not only Co 2p, Fe 2p, O 1s peaks, but also Mg 1s and Al 2p peaks, which also verified the formation of LDHs phase in the $CoFe_2O_4$ nanocomposite. In addition, the new peak at about 580.0 eV was detected from Fig. 7b, suggesting that adsorption of Cr(VI) on the adsorbent. Fig. 7c illustrated the high-resolution spectrum of O 1s for the virgin adsorbent. Devolution of the peak O 1s of $CoFe_2O_4$/MgAl-LDH clearly showed three components at binding energy of 532.6, 531.7 and 530.6 eV. The first component at binding energy of 532.6 eV was assigned to chemically or physically adsorbed water.[49] The second one, at about 531.7 eV, corresponded to hydroxyl groups as also identified in several other adsorbents such as iron nanoparticles,[49] Al_3Mg_2,[50] and Mg–Fe–La composite[51] at the same binding energy. The third one at binding energy of 530.6 eV was assigned to O^{2-} of Co, Fe, Mg and Al oxide (denoted as M–O, because Co, Fe, Mg and Al oxides could not be clearly separated).[51] Notably, the intensity and O 1s components of the adsorbent had obvious changes after Cr(VI) adsorption (Fig. 7d). Compared with the virgin

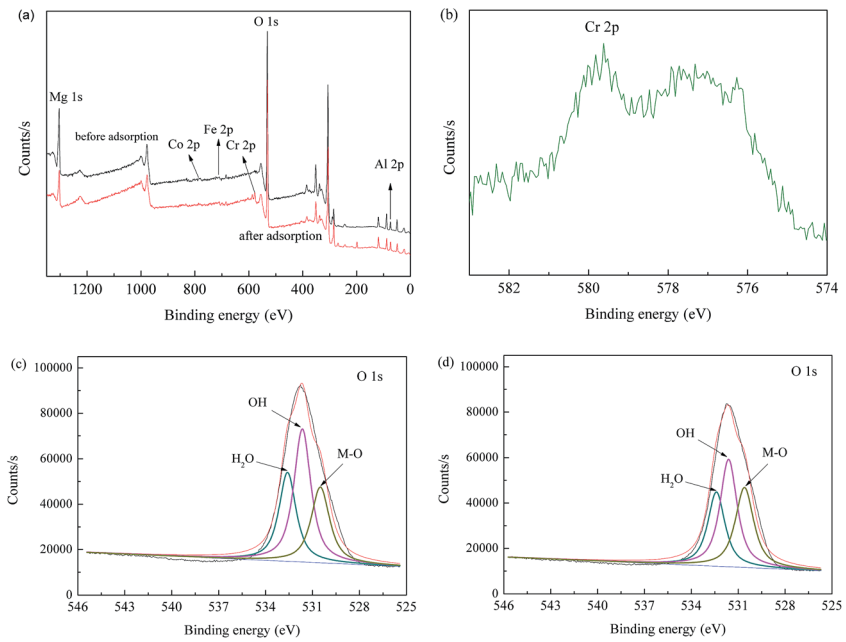

Fig. 7 Wide XPS spectra of (a) $CoFe_2O_4$/MgAl-LDH before and after Cr(VI) adsorption, (b) Cr 2p spectrum of $CoFe_2O_4$/MgAl-LDH after Cr(VI) adsorption, (c) O 1s spectrum of $CoFe_2O_4$/MgAl-LDH, and (d) O 1s spectrum of $CoFe_2O_4$/MgAl-LDH after Cr(VI) adsorption.

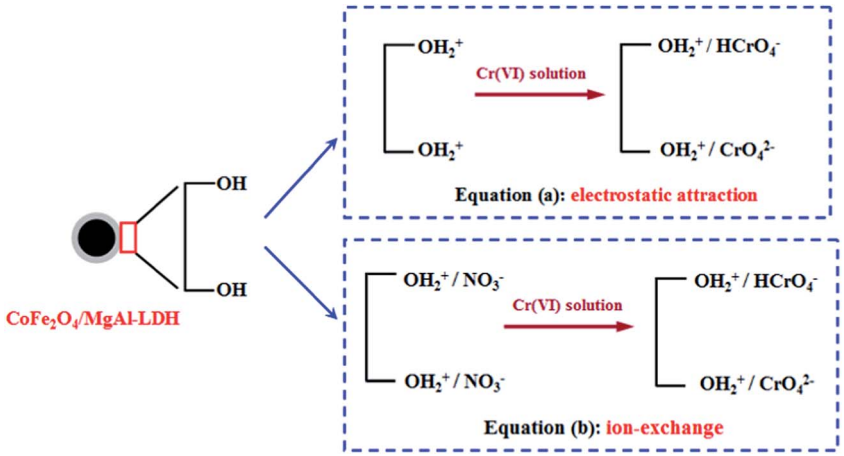

Fig. 8 Schematic illustration of the adsorption mechanism of Cr(VI) on $CoFe_2O_4$/MgAl-LDH.

$CoFe_2O_4$/MgAl-LDH, the relative area ratio for the peak assigned to M–O increased from 22.29% to 36.25%. However, the relative area ratio for the peaks corresponding to H_2O and OH decreased from 30.20% to 25.56% and from 47.51% to 38.19%, respectively, and this further revealed that hydroxyl groups on the adsorbent surface participates in the adsorption of Cr(VI).

In conclusion, the adsorption of Cr(VI) onto $CoFe_2O_4$/MgAl-LDH involved both physical and chemical adsorption and could be speculated to occur in two ways. On one hand, Cr(VI) ions entered and were adsorbed into the pores of the $CoFe_2O_4$/MgAl-LDH composite through physical adsorption. On the other hand, as shown in Fig. 8, adsorption occurred at the adsorbent surface *via* electrostatic interaction between negative charged Cr(VI) ions and positively charged surface of the $CoFe_2O_4$/MgAl-LDH composite, forming an outer-sphere complex. Moreover, NO_3^- anions existing in interlayer of the adsorbent were exchanged with Cr(VI) anions through anion exchange.

3.6 Effect of coexisting ions

Investigations showed that the concentrations of coexistent cations and anions in industrial wastewater containing Cr(VI) generated from electroplating, metal finishing, leather tanning, and pigment manufacturing varied from dozens to hundreds of milligrams per liter (mg L^{-1}). In this study, experiments were carried out to examine the effect of commonly present non-toxic ions such as Na^+, K^+, Ca^{2+} and Mg^{2+} (C_0 = 2000 mg L^{-1}), on removal of Cr(VI) by $CoFe_2O_4$/MgAl-LDH. It turned out that the presence of these kinds of cations have no significant influence on the removal efficiency of Cr(VI). As Cr(VI) exist in the form of anions in aqueous phase, and adsorption of Cr(VI) occurs at the adsorbent surface *via* electrostatic interaction and anion exchange in our study. Therefore, cations such as Na^+, K^+, Ca^{2+} and Mg^{2+} can not be adsorbed effectively by $CoFe_2O_4$/MgAl-LDH.

Experiments were also performed to study the effect of commonly present anions such as NO_3^-, Cl^-, SO_4^{2-} and PO_4^{3-} (C_0 = 200, 400, 800, 2000 mg L^{-1}) on Cr(VI) adsorption, and the results were depicted in Fig. 9. The removal of Cr(VI) using $CoFe_2O_4$/MgAl-LDH was inhibited by the addition of SO_4^{2-} and PO_4^{3-} in the solution, however, the inhibition effect of Cl^- and NO_3^- on Cr(VI) removal was negligible even when the concentration of Cl^- and NO_3^- was increased up to 2000 mg L^{-1}. Anions of SO_4^{2-} and PO_4^{3-} are known to be adsorbed by forming firmly bonded inner-sphere complex with the hydroxyl groups at the surface of adsorbents, however, NO_3^- and Cl^- could only form outer-sphere complex.[52,53] This indicated that Cr(VI) was adsorbed by forming inner-sphere complex on the surface of $CoFe_2O_4$/MgAl-LDH, and therefore SO_4^{2-} and PO_4^{3-} competed with Cr(VI) ions much better than NO_3^- and Cl^-.

3.7 Desorption and reusability study

To gain further insight into its actual application, the regeneration and reuse of $CoFe_2O_4$/MgAl-LDH was investigated using Na_2CO_3 (0.05 mol L^{-1}) as eluent (Fig. S5†). From the figure, it was found that the adsorbed amount of Cr(VI) on $CoFe_2O_4$/MgAl-LDH was still high in the sixth regeneration cycle, with 14.86

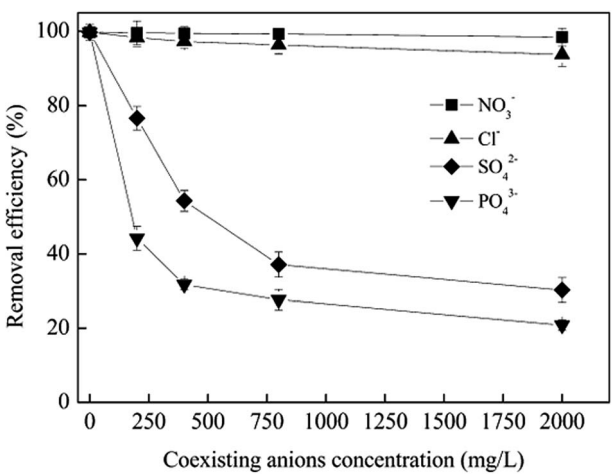

Fig. 9 Effect of coexisting anions on adsorption of Cr(VI) on $CoFe_2O_4$/MgAl-LDH.

mg g^{-1} of Cr(VI) adsorption which decreased only by 9.5% compared with the adsorbed amount in first cycle, suggesting that the as-prepared adsorbent could be regenerated and reused effectively by Na_2CO_3 and could have the potential use in treatment of wastewater contaminated by Cr(VI).

4. Conclusions

Magnetic $CoFe_2O_4$/MgAl-LDH composite was successfully prepared, well characterized by SEM, BET, XRD, FTIR and XPS, and employed as an adsorbent for Cr(VI) removal. The result showed that the synthesized $CoFe_2O_4$/MgAl-LDH was a composite of $CoFe_2O_4$ and MgAl-LDH, and the combination was a physical process. The BET surface area and average pore diameter of the adsorbent were 120.75 m^2 g^{-1} and 18.85 nm, respectively. Batch adsorption experiments showed that the adsorption of Cr(VI) using $CoFe_2O_4$/MgAl-LDH was dependent on solution pH, contact time, initial concentration, temperature and coexisting anions. The adsorption kinetics followed pseudo-second-order kinetic equation. The equilibrium data could be fitted by the Langmuir isotherm, and the maximum adsorption capacity was found to be 72.4 mg g^{-1} for temperature of 25 °C. Thermodynamic studies revealed the exothermic and spontaneous nature of the adsorption process. Mechanism study indicated that Cr(VI) adsorption on $CoFe_2O_4$/MgAl-LDH not only included physical adsorption on the adsorbent surface, but also involved the chemical adsorption of complexation and ion exchange interaction. These results indicated that the prepared $CoFe_2O_4$/MgAl-LDH was an effective adsorbent for Cr(VI) removal with quick separation.

Acknowledgements

This work was financially supported by the National Science & Technology Pillar Program during the Twelfth Five-year Plan Period (2012BAJ24B03).

References

1 B. Deng and T. S. Alan, *Environ. Sci. Technol.*, 1996, **30**, 2484.
2 Y. Y. Sun, Q. Y. Yue, Y. P. Mao, B. Y. Gao, Y. Gao and L. H. Huang, *J. Hazard. Mater.*, 2014, **265**, 191.
3 C. Weng, J. Wang and C. Huang, *Water Sci. Technol.*, 1997, **35**, 55.
4 B. Chen, X. S. Zhao, Y. Liu, B. G. Xu and X. J. Pan, *RSC Adv.*, 2015, **5**, 1398.
5 V. Sarin and K. K. Pant, *Bioresour. Technol.*, 2006, **97**, 15.
6 Ministry of Health, Sanitary Standard for Drinking Water, UDC 613.3/GB5749-2006, Ministry of Health, Beijing, 2006 (in Chinese).
7 R. C. Thomson and M. K. Miller, *Acta Mater.*, 1998, **46**, 2203.
8 S. Mustafa, K. H. Shah, A. Naeem, M. Waseem and M. Tahir, *J. Hazard. Mater.*, 2008, **160**, 1.
9 C. A. Kozlowski and W. Walkowiak, *Water Res.*, 2002, **36**, 4870.
10 E. Salazar, M. I. Oritiz, A. M. Urtiaga and J. A. Irabien, *Ind. Eng. Chem. Res.*, 1992, **31**, 1516.
11 J. N. Dui, G. Y. Zhu and S. M. Zhou, *ACS Appl. Mater. Interfaces*, 2013, **5**, 10081.
12 Y. Chen and G. Gu, *Bioresour. Technol.*, 2005, **96**, 1713.
13 X. Jing, Y. Gao, X. Zhang, D. Wang, X. Wu and H. Xu, *Desalination*, 2011, **269**, 120.
14 E. Demirbas, M. Kobya, E. Senturk and E. T. Ozkan, *Water SA*, 2004, **30**, 533.
15 S. J. Park and Y. S. Jang, *J. Colloid Interface Sci.*, 2002, **249**, 458.
16 A. B. Albadarin, C. Mangwandi, G. M. Walker, S. J. Allen, M. N. M. Ahmada and M. Khraisheh, *J. Environ. Manage.*, 2012, **114**, 190.
17 M. Avila, T. Burks, F. Akhtar, M. Gothelid, P. C. Lansaker, M. S. Toprak, M. Muhammed and A. Uheida, *Chem. Eng. J.*, 2014, **245**, 201.
18 L. Wang, X. Xu, D. G. Evans, X. Duan and D. Li, *J. Solid State Chem.*, 2010, **183**, 1114.
19 D. G. Evans and R. C. T. Slade, *Struct. Bonding*, 2006, **119**, 1.
20 S. L. Wang, R. J. Hseu, R. R. Chang, P. N. Chiang, J. H. Chen and Y. M. Tzou, *Colloids Surf., A*, 2006, **277**, 8.
21 Y. J. Li, B. Y. Gao, T. Wu, D. J. Sun, X. Li, B. Wang and F. J. Lu, *Water Res.*, 2009, **43**, 3067.
22 T. Kameda, E. Kondo and T. Yoshioka, *Sep. Purif. Technol.*, 2014, **122**, 12.
23 W. W. Wang, J. B. Zhou, G. Achari, J. G. Yu and W. Q. Cai, *Colloids Surf., A*, 2014, **457**, 33.
24 K. H. Goh, T. T. Lim and Z. L. Dong, *Water Res.*, 2008, **42**, 1343.
25 L. Deng, Z. Shi, B. Li, L. F. Yang, L. Luo and X. Z. Yang, *Ind. Eng. Chem. Res.*, 2014, **53**, 7746.
26 R. R. Shan, L. G. Yan, K. Yang, S. J. Yu, Y. F. Hao, H. Q. Yu and B. Du, *Chem. Eng. J.*, 2014, **252**, 38.
27 L. C. A. Oliveira, R. V. R. A. Rios, J. D. Fabris, V. Garg, K. Sapag and R. M. Lago, *Carbon*, 2002, **40**, 2177.
28 P. F. Wang, M. H. Gao, C. Wang, Y. H. Ao, J. Hou and J. Qian, *Appl. Surf. Sci.*, 2014, **290**, 116.
29 A. Mohammadi, H. Daemi and M. Barikani, *Int. J. Biol. Macromol.*, 2014, **69**, 447.
30 X. B. Fang, Z. Q. Fang, P. K. E. Tsang, W. Cheng, X. M. Yan and L. C. Zheng, *Appl. Surf. Sci.*, 2014, **314**, 655.
31 S. Z. Li, Y. B. Gong, Y. C. Yang, C. He, L. L. Hu, L. F. Zhu, L. P. Sun and D. Shu, *Chem. Eng. J.*, 2015, **260**, 231.
32 B. Tanhaei, A. Ayati, M. Lahtinen and M. Sillanpää, *Chem. Eng. J.*, 2015, **259**, 1.
33 J. Hu, I. M. C. Lo and G. H. Chen, *Langmuir*, 2005, **21**, 11173.
34 A. Pirouzfar and S. A. Seyyed Ebrahimi, *J. Magn. Magn. Mater.*, 2014, **370**, 1.
35 U. Costantino, F. Marmottini, M. Nocchetti and R. Vivani, *Eur. J. Inorg. Chem.*, 1998, **1998**, 1439.
36 L. W. Low, T. T. Teng, A. Ahmad, N. Morad and Y. S. Wong, *Water, Air, Soil Pollut.*, 2011, **218**, 293.
37 Y. S. Ho and G. McKay, *Process Biochem.*, 1999, **34**, 451.
38 S. S. Baral, S. N. Das and P. Rath, *Biochem. Eng. J.*, 2006, **31**, 216.
39 Z. Sadaoui, S. Hemidouche and O. Allalou, *Desalination*, 2009, **249**, 768.

40 V. K. Gupta, A. Rastogi and A. Nayak, *J. Colloid Interface Sci.*, 2010, **342**, 135.
41 Q. Cao, F. Huang, Z. Zhuang and Z. Lin, *Nanoscale*, 2012, **4**, 2423.
42 N. N. Das, J. Konar, M. K. Mohanta and S. C. Srivastava, *J. Colloid Interface Sci.*, 2004, **270**, 1.
43 E. Alvarez-Ayuso and H. W. Nugteren, *Water Res.*, 2005, **39**, 2535.
44 E. Ramos-Ramírez, N. L. Gutiérrez Ortega, C. A. Contreras Soto and M. T. Olguín Gutiérrez, *J. Hazard. Mater.*, 2009, **172**, 1527.
45 Y. F. Xu, J. Zhang, G. G. Qian, Z. P. Ren, Z. P. Xu, Y. Y. Wu, Q. Liu and S. Z. Qiao, *Ind. Eng. Chem. Res.*, 2010, **49**, 2752.
46 B. Houri, A. Legrouri, A. Barroug, C. Forano and J. P. Besse, *Collect. Czech. Chem. Commun.*, 1998, **63**, 732.
47 H. Liu, F. Xu, L. C. Li, Y. P. Wang and H. Z. Qiu, *React. Funct. Polym.*, 2009, **69**, 43.
48 H. H. Najafabadi, M. Irani, L. R. Rad, A. H. Haratameh and I. Haririan, *RSC Adv.*, 2015, **5**, 16532.
49 X. Q. Li and W. X. Zhang, *Langmuir*, 2006, **22**, 4638.
50 M. Liu, P. Schmutz, S. Zanna, A. Seyeux, H. Ardelean, G. Song, A. Atrens and P. Marcus, *Corros. Sci.*, 2010, **52**, 562.
51 J. Wang, D. J. Kang, X. L. Yu, M. F. Ge and Y. T. Chen, *Chem. Eng. J.*, 2015, **264**, 506.
52 C. H. Weng, C. Z. Tsai, S. H. Chu and Y. C. Sharma, *Sep. Purif. Technol.*, 2007, **54**, 187.
53 G. Lefèvre, *Adv. Colloid Interface Sci.*, 2004, **107**, 109.